Materials Today Bio 32 (2025) 101840

Contents lists available at ScienceDirect

Materials Today Bio

journal homepage: www.journals.elsevier.com/materials-today-bio

Superhydrophobic ROS biocatalytic metal coatings for the rapid healing of diabetic wounds

Jun Yu [a,1], Wu Duan [c,1], Jing Zhang [g,*], Ming Hao [h], Jie Li [f], Ruopu Zhao [f], Weikang Wu [f,**], Heng Han Sua [i], Hieng Kiat Jun [j,k,l], Yilun Liu [a], Yang Lu [d,e,***], Yang Liu [b,****], Sida Liu [a,*****]

[a] Laboratory for Multiscale Mechanics and Medical Science, SV LAB, School of Aerospace, Xi'an Jiaotong University, Xi'an, 710049, China
[b] Department of Hematology, Qilu Hospital, Cheeloo College of Medicine, Shandong University, Jinan, China
[c] Department of Endocrinology, Qilu Hospital of Shandong University, Jinan, 250012, Shandong, China
[d] Department of Mechanical Engineering, The University of Hong Kong, Hong Kong, China
[e] Materials Innovation Institute for Life Sciences and Energy (MILES), HKU-SIRI, Shenzhen, China
[f] Key Laboratory for Liquid-Solid Structural Evolution & Processing of Materials, Ministry of Education, Shandong University, Jinan, 250061, China
[g] Department of Cardiology, Shaanxi Provincial People's Hospital, Xi'an, 710068, Shaanxi Province, China
[h] School of Life Sciences, Tsinghua University, Beijing, 100084, China
[i] Schott Glass Malaysia, Perai, 13600, Malaysia
[j] Department of Mechanical and Materials Engineering, Lee Kong Chian Faculty of Engineering and Science, Universiti Tunku Abdul Rahman, Kajang, 43000, Malaysia
[k] Centre for Sustainable Mobility Technologies, Universiti Tunku Abdul Rahman, Kajang, 43000, Malaysia
[l] Centre for Advanced and Sustainable Materials Research, Universiti Tunku Abdul Rahman, Kajang, 43000, Malaysia

ARTICLE INFO

Keywords:
Diabetic wound healing
ROS
Intermetallic compound
Biocompatibility
Biomaterial
Biomechanics

ABSTRACT

In diabetic patients, hyperglycemia-induced elevated reactive oxygen species (ROS) accumulation severely impairs chronic wound healing by causing cellular component oxidation, inducing DNA damage, triggering cell death, exacerbating inflammatory responses, disrupting vascular endothelial function, reducing local blood supply, and inhibiting angiogenesis. This cascade results in a vicious cycle that delays the healing process. In this study, we developed a novel multifunctional composite dressing by depositing a transition-metal catalytic coating onto a superhydrophobic polydimethylsiloxane layer via magnetron sputtering. Two coatings were developed based on vanadium-ruthenium-boron (VRuB) intermetallic and VRu intermetallic compounds, which functioned as intermetallic compounds and exhibited various enzyme-like activities. The VRuB coating exhibited particularly prominent catalase-like activity (maximal reaction velocity (V_{max}) of 48.53 × 10^{-6} M s^{-1}; turnover number of 7.66 s^{-1}). Experimental characterizations and theoretical calculations revealed that B incorporation significantly improved catalytic performance. The artificial enzyme spray-coating process retained superhydrophobicity at the wound-contacting interface while enhancing the ROS-scavenging capabilities. Biological experiments demonstrated that the coating exhibited excellent biocompatibility and effective ROS-scavenging characteristics. These benefits were attributed to its synergistic properties, including its anti-adhesion characteristics, unidirectional drainage, moisturizing effects, and ROS elimination, which collectively promoted wound healing, especially for diabetic wound healing. The material showed promise for other applications requiring localized ROS scavenging while maintaining interfacial biomechanical properties.

* Corresponding authors.
** Corresponding authors.
*** Corresponding authors. Department of Mechanical Engineering, The University of Hong Kong, Hong Kong, China.
**** Corresponding author.
***** Corresponding author.
E-mail addresses: zjxjtu@126.com (J. Zhang), weikang_wu@sdu.edu.cn (W. Wu), ylu1@hku.hk (Y. Lu), liu-yang@mail.sdu.edu.cn (Y. Liu), sidaliu@xjtu.edu.cn (S. Liu).
[1] Jun Yu and Wu Duan contributed equally to this work.

https://doi.org/10.1016/j.mtbio.2025.101840
Received 23 February 2025; Received in revised form 1 May 2025; Accepted 4 May 2025
Available online 10 May 2025

1. Introduction

Reactive oxygen species (ROS) are oxygen-derived molecules produced during the metabolic processes of aerobic organisms [1]. ROS play a dual role in these organisms: at moderate, homeostatic levels, they participate in cellular signaling and maintain physiological balance [2], while excessive ROS levels can induce oxidative stress, damaging proteins, lipids, and DNA, ultimately leading to cellular dysfunction or death [3–7]. Elevated ROS levels are characteristic of infected and diabetic wounds, serving as a core factor underlying poor wound healing. In diabetic patients, hyperglycemia can cause osmotic imbalance, vascular dysfunction, neuropathy, and local infections, with ROS playing a central role. Hyperglycemia has been shown to significantly increase ROS levels, primarily through the activation of mitochondrial electron transport chains and oxidases. Concurrently, hyperglycemia can compromise the antioxidant defense system, reducing its capacity to eliminate ROS. At excessive levels, ROS adversely affect chronic wound healing by oxidizing cellular components, causing DNA damage and cell death, and exacerbating inflammatory responses. Inflammatory cells, such as neutrophils, release additional ROS, leading to endothelial dysfunction and increased immune cell infiltration, perpetuating a cycle of tissue damage, poor angiogenesis, and delayed healing [8]. Therefore, developing intervention strategies to target ROS is critical for managing diabetic and pressure ulcers, as well as other chronic wounds [3,9,10].

Current ROS control strategies primarily involve natural antioxidants, including enzymatic agents, such as superoxide dismutase and catalase [11], and non-enzymatic agents such as vitamins C and E [12]. However, natural enzymes suffer from instability, sensitivity to environmental factors, and production challenges [13–16]. To address these limitations, artificial enzymes that can mimic the ROS-scavenging activities of natural enzymes have attracted increasing interest [17]. Among transition-metal-based artificial enzymes, ruthenium (Ru) has demonstrated low electronegativity and stable redox properties, with the d-electron configuration of ruthenium enhancing its bonding capabilities, and its vacant orbitals optimizing its adsorption and desorption kinetics in redox reactions [18–20]. Modifying the d-electron configuration of the vanadium (V) center can change the adsorption energy between H_2O_2 and the metal site [21–23]. Furthermore, adding boron (B) can further modulate the catalyst's electronic structure, enhancing electron transfer efficiency and optimizing active site performance [24,25]. Various artificial enzymes have been developed, which can be categorized by their material dimensions [26]. These include zero-dimensional metal oxide nanozymes (i.e., Pd@CeO_2 [27]), one-dimension materials (i.e., carbon nanotubes [28]), two-dimension materials (i.e., V_2C MXenzyme [22]), and three-dimension materials (i.e., fullerol hydrogels [29] and Cu-assisted polydopamine nanoparticle hydrogels [30]).

Various immune cells participate in wound healing, with their accumulation leading to the secretion of a large number of inflammatory cytokines at the wound site, forming a chronic inflammatory environment that delays healing. Macrophages, in particular, play a crucial role in normal wound healing by promoting angiogenesis, collagen deposition, and tissue repair. Unlike normal wound healing, the wound healing mechanism of diabetic patients involves the overactivation of M1 macrophages and the impaired transition of macrophages from a pro-inflammatory M1 phenotype to an anti-inflammatory M2 phenotype [31,32]. Wound dressings based on new nanomaterials have shown significant promise in wound healing, enabling drug delivery, diagnostics, and intelligent responses to wound conditions [33]. We recently developed a sandwich-structured wound dressing (SWD) featuring a superhydrophobic polydimethylsiloxane (PDMS) layer that provided strong anti-adhesive properties against bacteria and granulation tissue. The SWD contained unidirectional drainage channels that effectively removed excess exudate while preventing backflow, maintaining a dry wound environment, and reducing infection risk [34,35]. However, the traditional incorporation of artificial ROS enzymes as nanoparticles or hydrogels may compromise the superhydrophobic surface of the SWD [36]. In this study, we developed a novel SWD with a transition-metal catalytic coating deposited on a superhydrophobic PDMS layer via magnetron sputtering. This innovative approach preserved the superhydrophobic properties of the wound contact surface and enhanced ROS scavenging at the wound interface.

Using physical vapor deposition, a functional VRuB coating was prepared through co-sputtering. As an intermetallic compound, VRuB possessed biocatalytic properties, exhibiting high ROS-scavenging efficiency and multiple enzymatic properties such as catalase (CAT) and superoxide dismutase (SOD) activities. The coating also exhibited nanoscale uniformity, abundant active sites, and a large specific surface area [37–39], which enhanced ROS-scavenging performance and maintained the biomechanical properties of the superhydrophobic surface. Experimental studies and density functional theory (DFT) calculations confirmed that the VRuB biocatalyst synthesized via magnetron sputtering exhibited CAT-like reaction kinetics similar to natural catalases, providing excellent performance compared with previously reported ROS-scavenging biocatalysts. Ex-vivo studies demonstrated that the modified coating reduced local ROS levels, accelerated healing, and preserved superhydrophobic properties, creating an antioxidant microenvironment conducive to cell regeneration. As a result, this novel VRuB coating could serve as a promising solution for treating diabetic chronic wounds (Scheme 1).

2. Results and discussion

2.1. Microstructure and composition analysis of the VRuB biocatalytic coating

A novel VRuB biocatalytic coating was developed in this study to enable the rapid and scalable deposition of coatings on medical material surfaces with high-efficiency ROS catalytic properties. Magnetron sputtering was chosen as the high-throughput method for the simultaneous deposition of VRuB coatings with various compositions. The atomic proportions of the coatings were also determined by inductively coupled plasma (ICP) analysis (Fig. S1), with the results revealing the successful incorporation of B, forming compounds such as $V_{65}Ru_{27}B_8$ and $Ru_{72}V_{21}B_7$. Among these compounds, $V_{68}Ru_{25}B_7$ exhibited balanced catalytic performance and stability, with the added advantage of cost-effectiveness. Scanning electron microscopy (SEM) (Fig. 1a and S2a, b) revealed a well-developed microstructure characterized by a rough surface morphology, which enhanced the surface area and provided abundant catalytic active sites, improving catalytic performance. The coating exhibited a characteristic columnar crystal structure with a uniform thickness (Fig. 1b). The coating also exhibited excellent adhesion on various medical substrates (Figure S2a, c), highlighting its potential for various medical material applications. In addition, the coating exhibited superhydrophobic properties (contact angle >150°) and retained its superhydrophobic characteristics even after bending tests (Figures S3). Therefore, the biomechanical characteristics of the coating played a key role in promoting wound healing.

Energy-dispersive X-ray spectroscopy (EDS) analysis revealed the spatial distributions of V and Ru, along with trace amounts of B, which were uniformly embedded in the VRu crystal matrix, confirming their successful incorporation (Fig. 1c). High-angle annular dark-field scanning transmission electron microscopy (HAADF-STEM) (Fig. 1d and S4) revealed the highly ordered crystalline arrangement of the coating with a lattice spacing of 0.2216 nm, consistent with the body-centered cubic (BCC) structure of VRu. Fast Fourier transform (FFT) analysis further validated the structural integrity. Notably, the inclusion of B did not disrupt the VRu crystal framework, and X-ray diffraction (XRD) (Figure S5) and HAADF-STEM imaging (Figure S6) confirmed the structural stability of the VRu crystal after B doping.

Notably, DFT calculations revealed that B incorporation preferentially occurred via interstitial doping instead of substitutional doping

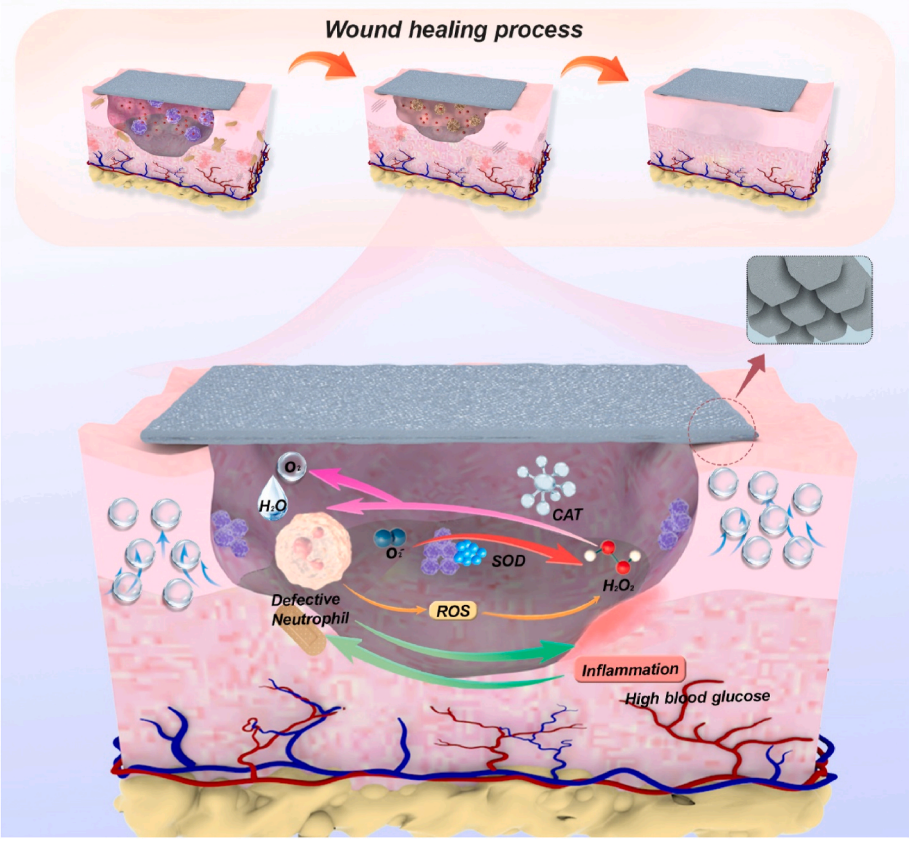

Scheme 1. Illustration of the working mechanism of intermetallic compound biocatalytic coating for ROS scavenging, stem cell protection and diabetic wound healing.

(Table S1). This aligned with the experimental results, demonstrating that the original VRu structure remained intact. Subsequent tests further revealed that B incorporation preserved the integrity of the original crystal structure and enhanced the catalytic performance of the material.

2.2. Performance evaluation of the VRuB coating in ROS catalysis

Following confirmation of the chemical and electronic structures of the VRuB biocatalytic coating, we systematically assessed the performance of the coating to determine its catalytic properties in ROS processing. The catalytic activities of the VRuB and VRu coatings were examined, which revealed that they exhibited significant effects in catalyzing reactive species such as H_2O_2, O_2^-, and 2,2-diphenyl-1-picrylhydrazyl radicals (DPPH·) (Fig. 2a). CAT-like activity was initially assessed using a titanium-peroxide complex method to measure H_2O_2 decomposition. The results indicated that the VRuB biocatalyst achieved up to 89.4 % H_2O_2 removal efficiency, surpassing the 75.2 % efficiency observed for the VRu biocatalyst, suggesting that B incorporation significantly enhanced catalyst activity.

Oxygen generation experiments also confirmed the performance of VRuB and VRu in decomposing H_2O_2 to release oxygen (Fig. 2b–S7, and S8). To assess the catalyst's mechanical properties, the VRuB coating was subjected to nanoindentation testing. The coating demonstrated favorable hardness and elastic modulus values during indentation, with no significant fluctuations in the curve, suggesting strong adhesion between the coating and the substrate (Figure S9). To evaluate the stability of the catalyst, at least 10 cycling tests were conducted (Fig. 2c and S10), along with bending tests. Small variation in the amount of coating shedding and some differences in performance (Figures S11–13). The results revealed that the coating showed no significant decline in catalytic performance following multiple uses, demonstrating its exceptional stability and highlighting its long-term durability for ROS-scavenging applications. Moreover, thickness-independent verification was conducted for the VRuB coating, showing that the coating thickness does not affect its catalytic performance or hydrophobicity (Figures S14, S15). In the steady-state catalytic kinetics study, the K_m, V_{max}, and turnover number (TON) values of VRuB were calculated (Figure S16). The V_{max} of VRuB reached 48.53 μM s^{-1}, with a TON value of 7.66 s^{-1}, and both of these values were significantly higher than those of VRu (Figure S17). These results indicated that VRuB demonstrated higher efficiency in catalytic kinetics similar to CAT, and the incorporation of interstitial B enhanced catalytic activity (Figure S18). As a novel intermetallic-compound-coated catalyst, the CAT-like enzymatic activity of the VRuB biocatalyst, with reaction kinetics similar to natural catalase (Figure S19), was substantially greater than that of conventional metal nanoparticle biocatalysts. The V_{max} and TON values of the VRuB biocatalyst were compared with those of existing nanoparticle-based metal biocatalysts, such as Mn_3O_4 and $Cu_{5.4}O$ (Fig. 2d and Table S2). The results showed that the VRuB biocatalyst exhibited excellent CAT-like activity and an outstanding TON value compared with other catalysts. In addition to CAT-like catalytic activity, the SOD-like activity of the VRuB biocatalyst was explored. SOD plays a crucial role in anti-ROS systems by scavenging superoxide radicals ($\cdot O_2^-$). Using the nitrotetrazolium blue chloride method, we found that the VRuB and VRu biocatalysts both demonstrated effective $\cdot O_2^-$ scavenging (approximately 75 % within 5 min (Fig. 2a and S20)), indicating that B incorporation did not alter the inherent SOD-like activity. Furthermore, a DPPH· radical scavenging assay was conducted to assess the reactive nitrogen species (RNS) scavenging capabilities of the biocatalyst. The VRuB biocatalyst exhibited advantageous performance in DPPH· scavenging, significantly outperforming the undoped VRu biocatalyst

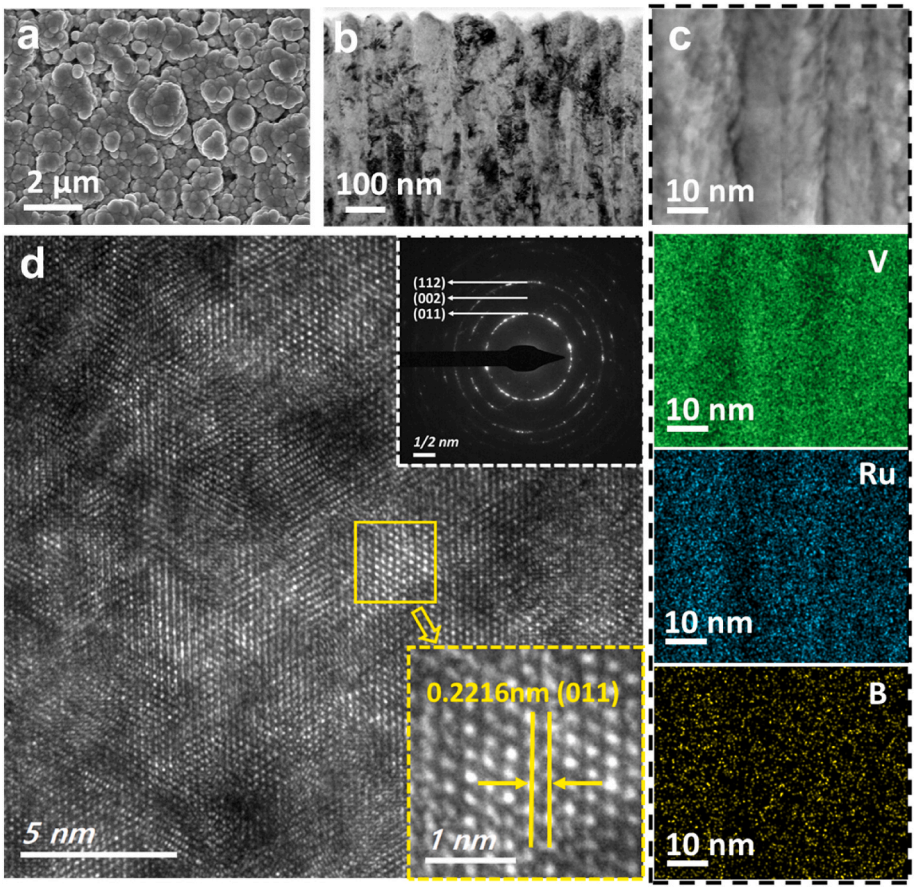

Fig. 1. Structural characteristics of biocatalytic coating. (a) SEM image of VRuB. (b) TEM image of VRuB. (c) STEM spectral imaging of the VRuB coating, illustrating the distribution of V, Ru, and B elements. (d) HAADF-STEM image showing the atomic arrangement of VRuB, with the white area in the upper right corner representing the selected area electron diffraction (SAED) pattern and the yellow area in the lower right corner showing a magnified view of the yellow box region in the image.

(Fig. 2a and S21). In summary, we observed that the VRuB biocatalyst surpassed the VRu biocatalyst in terms of CAT-like catalytic performance and exhibited enhanced SOD-like activity and RNS scavenging ability due to the incorporation of B. This unique multifunctional activity highlighted the potential application of the VRuB biocatalyst in ROS management, offering new insights for the design of advanced biocatalysts.

2.3. Chemical and electronic structure characterization of the VRuB biocatalytic coating

To elucidate the chemical and electronic structures of the VRuB biocatalytic coating, a comprehensive X-ray photoelectron spectroscopy (XPS) assessment was conducted (Fig. 3a–c and S22). The XPS spectra prominently contained signals for V, Ru, and B, confirming the successful integration of B in the VRu crystal, with stable dispersion throughout the material. Notably, significant negative shifts were observed in the V 2p and Ru 3p peaks of the VRuB sample relative to the undoped VRu sample, highlighting the electronic influence of B doping. An in-depth analysis of the V 2p peak revealed that V was primarily present in a metallic V^0 state, accompanied by minor oxidized species. B incorporation induced a −0.19 eV shift in the V 2p peak, suggesting an increase in local electron density and resulting reduction in binding energy. Notably, peak area analysis indicated no substantial change in the proportion of oxidized V species (Figure S23a). A more pronounced −0.21 eV shift in the Ru 3p peak suggested that B integration notably changed the electronic environment of Ru, likely increasing its oxidation state. This hypothesis was further validated by peak area analysis (Figure S23b). The B 1s spectrum indicated that B was predominantly present in a B^0 state, with some negatively charged species, implying the formation of Ru–B bonds. The formation of this bond indicated that B was structurally integrated into the VRu crystal and endowed the material with distinct electronic characteristics, enhancing its potential catalytic capabilities.

X-ray absorption spectroscopy (XAS) analysis was performed to further elucidate the detailed coordination structure and electronic state of the VRuB biocatalyst, with a specific emphasis on the Ru K-edge X-ray absorption near-edge structure (XANES). The coordination environment of Ru in the biocatalyst was found to closely align with that of the Ru foil, effectively eliminating significant oxidation. The XANES spectrum revealed that the Ru K-edge pre-edge peak of the biocatalyst was positioned between those of the Ru foil and RuO_2, indicating that the Ru atoms present in the biocatalyst were in a partially oxidized state (Fig. 3d). Valence state analysis further confirmed this partial oxidation, with an average Ru valence state near 1.9 (Fig. 3e), consistent with the XPS data. The k^2-weighted Fourier-transformed extended X-ray absorption fine structure spectroscopy (FT-EXAFS) curves revealed the presence of Ru–B, Ru–V, and Ru–Ru bonds in the biocatalyst. The coordination peaks around 2 Å for Ru–B and Ru–V distinguished the biocatalyst from the pure Ru foil, where Ru–Ru coordination was dominant (Fig. 3g and S24). This shift suggested that the local chemical environment around the Ru atoms was significantly modified through the incorporation of B and V. Supporting this, the fitting results demonstrated a reduction in the Ru–Ru coordination number from 12 to 1.8 ± 0.3, while the Ru–B and Ru–V coordination numbers increased to 1.7 ± 0.2 and 3.0 ± 0.2, respectively (Table S3). Wavelet transform (WT)

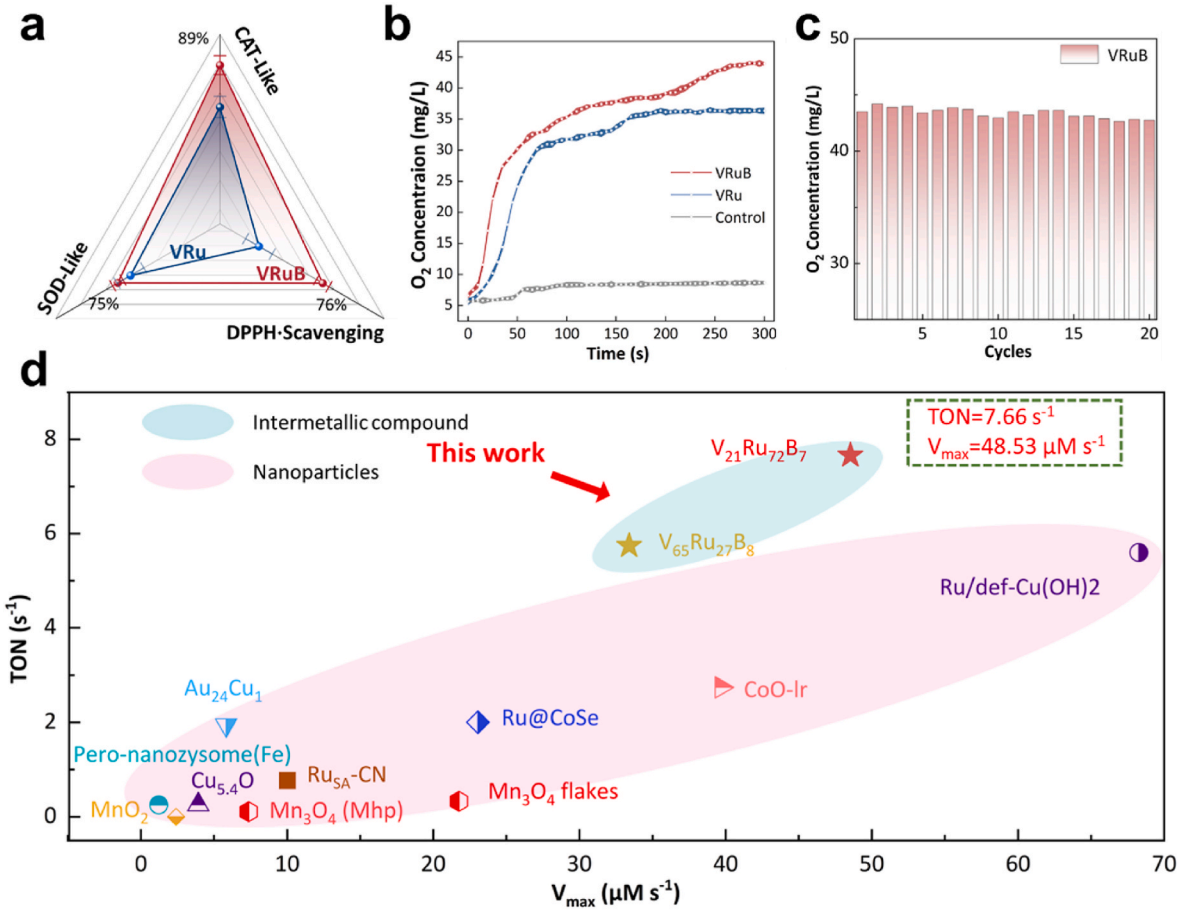

Fig. 2. Biocatalytic ROS scavenging properties of biocatalytic coating. (a) Radar chart of the biocatalytic ROS scavenging properties. (b) CAT-like activity of VRu and VRuB demonstrated through O_2 generation (c) Stability testing of the CAT-like activity of VRuB. (d) Comparison of the TON and V_{max} values of the prepared biocatalyst with those of other established biocatalysts, as referenced in Table S3. (In a and b, n = 3 independent experiments, Data were expressed as mean ± S.D.)

analysis was applied (Fig. 3h–j) for detailed characterization of the Ru species to obtain a better understanding of the distribution of the coordination structures in the biocatalyst. Distinct coordination features of Ru–B, Ru–V, and Ru–Ru in the biocatalyst were evident in the WT images. Compared with the coordination profiles of the Ru foil and RuO_2, the biocatalyst exhibited prominent coordination peak intensities. These coordination signals confirmed the influence of B and V on Ru's local environment and underscored the close association between Ru's partial oxidation state and its coordination with B.

Further DFT calculations confirmed that B doping significantly regulated the electronic structure of the biocatalyst. The partial density of states (PDOS) analysis showed a noticeable shift of the d-band center closer to the Fermi level (Fig. 3f and S25). This shift enhanced the coupling between d-electrons and adsorbates, improving the adsorption capacity for reactants and significantly boosting the catalytic performance. A d-band center closer to the Fermi level indicated that d-orbital electrons were more readily available for chemical bonding, effectively lowering the reaction activation energy. Moreover, Bader charge analysis revealed an increase in the charge of B atoms (Figure S26), indicating that doping induced electronic redistribution, optimizing the electronic properties of the active sites. The catalytic reaction pathway was also calculated, and the rate-determining step was found to have an energy barrier of 8.366 eV (Figure S27, Table S4). These findings highlight that tuning the d-band center position through doping is a crucial strategy for enhancing the catalytic activity, offering new insights for designing highly efficient catalysts.

2.4. Evaluation of material biocompatibility

To evaluate the biocompatibility of the VRuB biocatalyst, dose-dependent cytotoxicity tests were conducted using human mesenchymal stem cells (hMSC), mouse embryonic fibroblasts (NIH-3T3), human umbilical vein endothelial cells (HUVEC), and the human keratinocyte cell line (HaCaT), all of which play important roles in wound healing. The VRu and VRuB catalysts were coated on 9 mm glass coverslips at a dosage of 20 μg per coverslip, and the coated (experimental) and uncoated (control) coverslips were co-cultured with cells for 24, 48, and 72 h. Cytotoxicity was assessed using cell-counting kit-8 (CCK-8) and lactate dehydrogenase (LDH) assays, with the results showing no significant difference in cell viability between the experimental and control groups. The proliferation rates of cells in each group were similar (Figure S31), and no significant increase in cytotoxicity was observed over time.

Live/dead cell assays were also conducted by incubating hMSC, NIH-3T3, HUVEC, and HaCaT cells with VRuB-coated 48-well glass coverslips for 48 h. Cell viability was assessed using fluorescence microscopy, with live cells stained with acridine orange (AO, green) and dead cells stained with propidium iodide (PI, red). No significant differences were observed between the groups, indicating that the coated materials did not exhibit cytotoxic effects (Figure S32). In addition, dose-related effects on the cell viability were evaluated using CCK-8 and LDH assays, where different doses of VRu and VRuB were added by increasing the number of coated coverslips per well. After 24 h, no significant inhibition of the cell viability was observed in any dose group.

In summary, the VRu and VRuB biocatalysts demonstrated

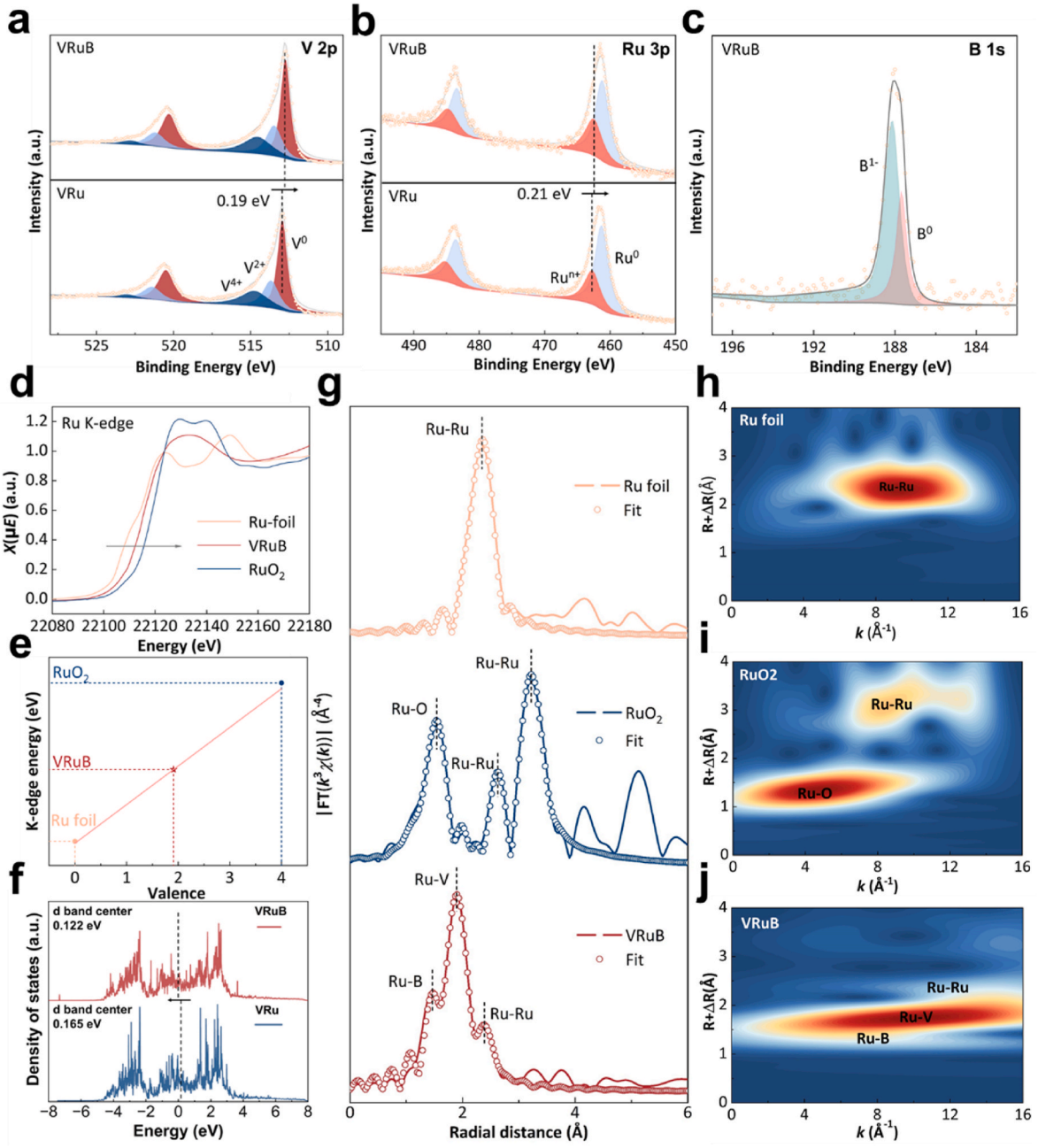

Fig. 3. Electronic structure and chemical analysis of VRuB. (a–c) XPS analysis of the biocatalyst: (a) V 2p, (b) Ru 3p, and (c) B 1s. (d) XANES spectra at the Ru K-edge for VRuB, Ru foil, and RuO_2. (e) Average valence states of Ru for VRuB, Ru foil, and RuO_2. (f) Comparison of PDOS for VRu and VRuB (g) Fourier transform of the k^2-weighted χ(k) function in R-space and the fitted curves for VRuB, Ru foil, and RuO_2. (h–j) WT of the k^2-weighted Ru K-edge EXAFS signals for VRuB, Ru foil, and RuO_2.

satisfactory cell compatibility with hMSC, NIH-3T3, HUVEC, and HaCaT cells in a 2 mL culture system, with loading amounts ranging from 20 to 60 μg/cm^2. These favorable results provide a solid foundation for future in-vivo studies.

2.5. *Ex vivo toxicity evaluation in mice*

We subsequently conducted an ex vivo evaluation of the biocompatibility of the VRu and VRuB surface biocatalysts. Our previous studies had already validated the safety and efficacy of PDMS membranes as wound dressings. In the animal experiments, VRu or VRuB surface biocatalysts were sprayed onto the PDMS membrane to decrease wound exudate and degrade ROS through surface catalysis. After covering the wounds with VRu- or VRuB-coated PDMS membranes for 15 days, the mice were euthanized, and major organs (heart, liver, spleen, lung, and kidney) were harvested for H&E staining and pathological analysis. Firstly, ICP analysis was performed on mouse tissue samples at day 0 and day 15. No coating elements were detected in either sample (Table S5). And no obvious organ damage, histological abnormalities, or inflammatory lesions were observed in the H&E-stained images of the heart, liver, spleen, lung, and kidney in any of the treated groups, indicating that all prepared dressings were non-toxic and biologically safe (Figure S33).

Further, serum biochemical analyses were conducted by collecting blood from the retro-orbital sinus of the mice. The biochemical parameters, including alanine transaminase (ALT), aspartate transaminase

(AST), AST/ALT ratio, alkaline phosphatase (ALP), gamma-glutamyl transferase (γ-GT), blood urea nitrogen (BUN), creatinine (CREA), uric acid (UA), total bilirubin (TBIL), direct bilirubin (DBIL), total protein (TP), and albumin (ALB), showed no significant differences among the groups (Figure S34). This further confirms that the application of VRu- or VRuB-coated PDMS membranes (VRu-PDMS, VRuB-PDMS) had minimal side effects on the serum biochemical indicators of the experimental mice, demonstrating good biocompatibility of the two dressings and minimal adverse effects on liver and kidney function and metabolism.

2.6. Protection of cells from ROS damage by the VRuB biocatalyst

To evaluate the capability of the VRuB catalyst in protecting cells from ROS-induced damage, we conducted multiple experiments. Initially, intracellular ROS levels in hMSC, NIH-3T3, HUVEC, and HaCaT cells were quantified using 2,7-dichlorofluorescein diacetate (DCFH-DA) in media containing H_2O_2. The positive control group (100 μM H_2O_2) showed a strong green signal, indicating high ROS levels. When VRu- or VRuB-coated glass coverslips were added to the H_2O_2-containing media, the intracellular ROS signals were significantly reduced, particularly in the VRuB group, where the ROS levels were markedly lower (Fig. 4a). Quantitative analysis (Fig. 4b and c) confirmed that the VRuB group had the lowest ROS levels, significantly lower than the VRu group,

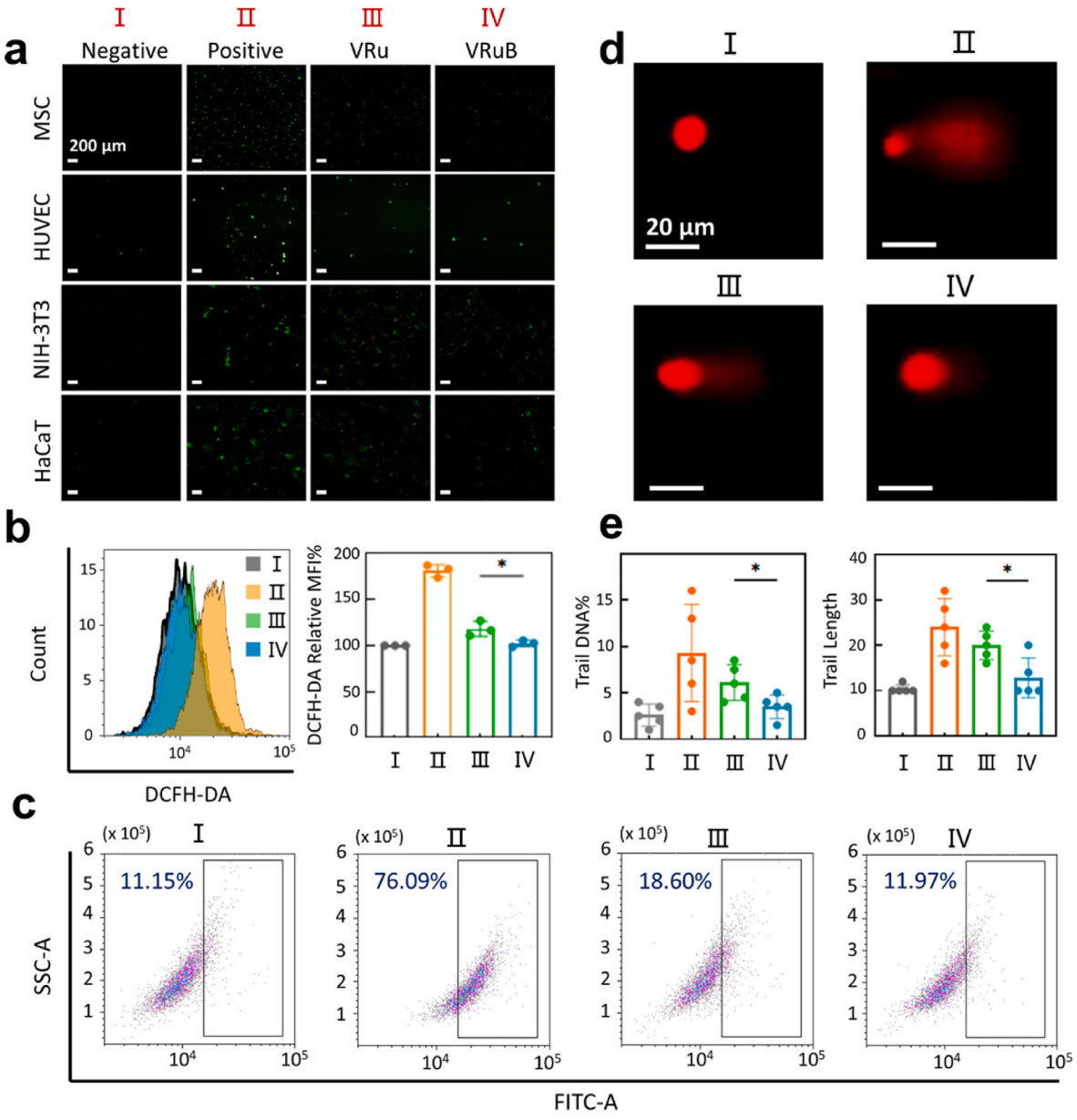

Fig. 4. Biocatalytic coatings protects cells from ROS-induced damage. (a) Schematic representation of the hMSC culture system exposed to 100 μM H_2O_2 to simulate high ROS conditions. After treatment with VRu or VRuB-coated coverslips, intracellular ROS levels were measured using DCFH-DA, revealing a significant reduction in ROS levels in both VRu and VRuB groups, with VRuB showing superior ROS scavenging ability. I, negative group; II, positive group (100 μM H_2O_2); III, VRu-treated group; IV, VRuB-treated group. (b–c) Flow cytometry analysis showing ROS levels in different treatment groups, with quantitative statistics on the reduction of ROS following VRu and VRuB treatment. (d) Comet assay to assess DNA damage induced by ROS. The 100 μmM H_2O_2 positive control exhibited a long tail composed of DNA fragments, indicative of typical DNA damage, while the VRu group showed a shorter tail, suggesting reduced DNA damage. The VRuB group presented a compact, circular signal, suggesting minimal DNA damage. (e) Quantitative evaluation of DNA damage by tail DNA percentage and tail length, with the VRuB group showing values closest to the negative control group.

demonstrating superior ROS scavenging ability.

To further assess DNA damage, we performed comet assays. The positive control group (100 μM H_2O_2) exhibited long DNA fragments with tails, indicating substantial DNA damage (Fig. 4d). In contrast, the VRu group showed shorter and less intense tail signals, suggesting reduced DNA damage, while the VRuB group displayed minimal DNA damage with compact, round signals. Quantitative analysis (Fig. 4e) confirmed these observations, with the VRuB group showing significantly reduced DNA damage compared to the VRu group. These results indicate that the VRuB catalyst not only scavenges ROS but also effectively reduces ROS-induced DNA damage, protecting the cells' genetic integrity.

To investigate ROS-related cell death, live/dead assays were conducted after incubating cells in media containing 100 μM H_2O_2. The VRu

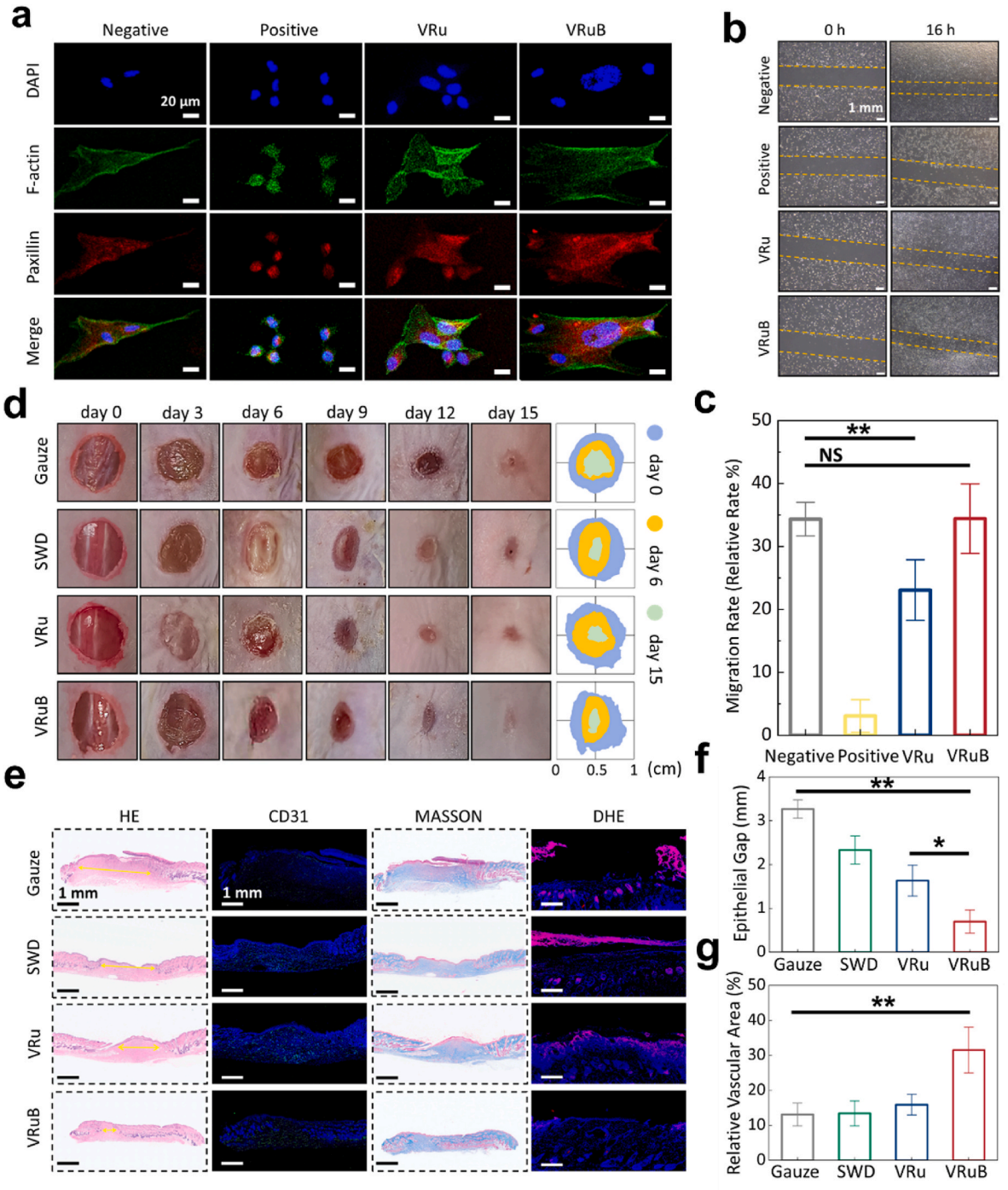

Fig. 5. Catalyst-mediated protection of cell function under high ROS conditions. (a) hMSC expansion assessment with Pallixin and F-actin staining under high ROS environment induced by 100 μM H_2O_2. Green: F-actin, red: Paxillin, blue: dapi. (b) Cell scratch assays were performed using hMSC cells to evaluate the effects of H_2O_2 and different catalysts on cell proliferation and migration. The observation time points for each cell type were adjusted based on their respective proliferation rates. (c) Quantitative analysis of migration rate in the cell scratch assay. (d) The evolution of the wounds treated with gauze (control), SWD, VRu-SWD, and VRuB-SWD, respectively. (e) H&E, CD31, Masson's and DHE staining of the skin tissue around wounds. H&E, CD31, and Masson's staining were performed on paraffin sections, while DHE staining was conducted on frozen sections. (f) The histological epithelial gap measurement of the skin tissue around wounds. (g) Angiogenesis quantified by the percentage of CD3l-positive area to total DAPI area.

and VRuB groups exhibited significantly lower cell death rates compared to the positive control group, with the VRuB group showing cell death rates similar to the negative control group (Figure S35). These results suggest that VRuB plays a crucial role in protecting cell membrane integrity and preventing cell death in high-ROS environments.

After confirming the protective effects of the VRuB biocatalyst against ROS-induced DNA damage and cell death, we assessed its impact on stem cell function, specifically focusing on cell spreading and morphology. In the H_2O_2-treated positive control group, stem cells showed poor spreading, rounded morphology, and few protrusions. In contrast, cells incubated with VRu or VRuB catalysts exhibited good spreading, flat spindle-shaped morphology, and well-organized protrusions (Fig. 5a). Paxillin expression, which is a marker of focal adhesions (FAs), was reduced under high ROS conditions (Fig. 5a). In cells treated with the VRu or VRuB biocatalyst, paxillin expression was restored, with visible FA distribution at the periphery, suggesting that VRu and VRuB effectively rescued the ability of hMSC to maintain cytoskeletal remodeling, cell morphology, and adhesion in high-ROS environments.

We also evaluated the protective effects of VRuB on cell migration function, which is critical in diabetic conditions where high ROS levels impair cell migration. Using cell scratch assays, we assessed migration in hMSC, NIH-3T3, HUVECs, and HaCaT cells. In the H_2O_2-treated group, migration was significantly inhibited compared to the negative control group, but the introduction of catalyst-coated coverslips counteracted this effect (Fig. 5b and c). The VRuB group exhibited significantly better protection against ROS-induced migration inhibition compared to the VRu group. In the H_2O_2 group, marked cell detachment and death were observed, while in the VRuB group, cell detachment and apoptosis were rare. This suggests that VRuB's superior ROS-scavenging capability reduces the exposure to high ROS levels and protects cells from damage. Over a prolonged treatment period (12–24 h), hMSC and HUVEC migration and proliferation gradually improved in the VRu group, likely due to the decreased H_2O_2 concentration and the recovery of surviving cells. However, NIH-3T3 cell migration and proliferation did not recover, possibly due to different sensitivities of these cells to ROS (Figure S36).

These findings confirm that the VRuB catalyst excels in protecting a variety of cells involved in wound healing from ROS-induced damage, demonstrating broad, non-specific protective effects.

2.7. Enhancement of wound healing in diabetic mice using VRuB-coated composite dressings

Building on our earlier findings regarding the anti-adhesive functionality of the SWD and the protective effects of the catalytic coating on cell proliferation following ROS clearance, we initiated animal studies in mice to assess the influence of various fabricated dressings on wound healing. The VRuB and VRu catalysts were sprayed onto the innermost superhydrophobic PDMS layer of the SWD to develop ROS-scavenging versions, designated as VRuB-SWD and VRu-SWD.

In the diabetic wound model on the mouse's back (Fig. 5d–S37), wounds were treated with different dressings: gauze control, SWD, VRuB-SWD, and VRu-SWD. The wound healing process was monitored over 15 days, with dressings changed every 3 days. During the early inflammatory phase (0–6 days), the VRuB-SWD group demonstrated significantly faster healing, fewer infections, and better overall healing quality compared to the gauze control and SWD groups. In the proliferative phase (6–12 days), both VRu-SWD and VRuB-SWD groups exhibited more active dermal proliferation. By the remodeling phase (12–15 days), the VRuB-SWD group achieved the earliest completion of skin healing and re-epithelialization, accompanied by regeneration of skin appendages and regression of newly formed blood vessels.

To evaluate the quality of wound healing and clarify the anti-ROS effects, we performed histological analysis, including HE staining, Masson's trichrome staining, CD31 immunofluorescence, DHE staining, and macrophage M1/M2 polarization immunofluorescence analysis (Fig. 5g–S38-S39). The gauze control group showed poor healing, with irregular wound edges due to tissue detachment during dressing changes (Fig. 5e and f). The DHE staining of the gauze group showed significant detachment of loose wound tissue, while the porous gauze structure allowed granulation tissue to grow into the pores, causing severe adhesion and leading to tissue detachment during dressing changes. This resulted in wrinkles and scars in the healed wound, as indicated by excessive collagen deposition in Masson's trichrome staining, which can lead to hypertrophic keloid formation. In contrast, the SWD group, which reduced adhesion, exhibited a more even wound surface and faster healing but with less collagen deposition due to the absence of additional healing interventions.

In the VRu and VRuB groups, the catalytic ROS metal coatings were applied using magnetron sputtering, effectively preserving the anti-adhesive properties of the SWD. The introduction of these ROS-scavenging catalysts significantly reduced wound ROS levels, as shown by DHE staining (Fig. 5e and f), and corrected the high local ROS state. In the VRuB group, the more potent ROS scavenging capability of VRuB effectively eliminated excessive ROS, with DHE staining showing almost no red fluorescence. CD31 staining (Fig. 5e and f) demonstrated that reduced ROS production improved the diabetic wound microenvironment, mitigating oxidative stress and enhancing local angiogenesis, which is critical for effective wound healing. Macrophage polarization analysis by immunofluorescence (CD86+M1/CD206+M2) revealed that ROS reduction induced significant attenuation of pro-inflammatory M1 macrophages, particularly in the superficial wound bed, thereby rectifying the detrimental inflammatory milieu (Figure S39).

These findings demonstrate that the VRuB-SWD not only maintains the anti-adhesive effects of the SWD dressing but also protects against oxidative stress, promoting dermal fibroblast proliferation, migration, and angiogenesis, leading to accelerated healing of diabetic wounds.

2.8. Prospects for clinical applications

The VRuB-SWD developed in this study has demonstrated significant advantages in the healing of diabetic wounds, underscoring its important clinical application potential. This material also holds broad application prospects in other scenarios where local ROS clearance and maintenance of interfacial biomechanical properties are required, such as within implanted arteriovenous catheters. In these settings, it is critical to clear ROS while maintaining the catheter's anti-adhesive, anti-platelet, anti-thrombotic, and antibacterial properties at the blood interface. The development of this efficient ROS-scavenging catalyst in a coating form represents a novel and promising approach to drug delivery. It has the potential for widespread use in conditions related to ROS, including the promotion of ulcer healing in diabetes and the prevention of thrombus formation in blood vessels.

3. Conclusions

In this study, we successfully fabricated a VRuB bio-ROS catalytic metal coating via magnetron sputtering. As an intermetallic compound, the coating was stable and exhibited multiple enzyme-like activities, with particularly prominent CAT-like activity (V_{max}: 48.53 μM/s; TON: 7.66 s^{-1}). Structural analysis showed no significant changes in the coating's structure following B incorporation compared to the original VRu coating. Characterization and DFT calculations revealed that B incorporation enhanced the proportion of oxidized Ru species, forming stable bonds with Ru, lowering the d-band center, and ultimately leading to significantly improved catalytic performance. Biological experiments demonstrated that the coating exhibited excellent biocompatibility, effectively scavenging ROS, protecting the cells from high-ROS-induced damage, and significantly reducing DNA damage, thus maintaining genomic integrity. In addition, the coating promoted cytoskeletal remodeling, preserved cell morphology, and enhanced cell

adhesion in hMSC. These properties were attributed to the synergistic effects of the coating's early-stage anti-adhesion capability, including unidirectional drainage, moisturizing performance, and ROS-scavenging function, which collectively facilitated wound healing. Moreover, the coating could withstand the sterilization process without significantly losing its catalytic activity or mechanical stability. In addition, the VRuB-SWD coating demonstrated significant advantages for diabetic wound healing, highlighting its great clinical potential. Furthermore, this material demonstrated promise in applications requiring localized ROS scavenging while maintaining interfacial biomechanical properties, such as arterial and venous catheter coatings. In these scenarios, it could effectively scavenge ROS while preventing adhesion, platelet aggregation, thrombosis, and bacterial infections at the blood-material interface. This high-performance ROS-scavenging catalytic coating represents a novel and promising approach for treating ROS-related diseases, with broad potential in applications such as diabetic wound healing and thrombosis prevention. In the future, we will focus on improving the compatibility of the coating with existing wound care frameworks and further controlling costs associated with the coating.

CRediT authorship contribution statement

Jun Yu: Writing – original draft, Software, Methodology, Investigation, Formal analysis, Data curation, Conceptualization. **Wu Duan:** Validation, Software, Methodology, Investigation, Funding acquisition, Formal analysis. **Jing Zhang:** Supervision, Methodology, Data curation. **Ming Hao:** Validation, Formal analysis. **Jie Li:** Formal analysis, Data curation. **Ruopu Zhao:** Software, Formal analysis. **Weikang Wu:** Supervision, Project administration. **Heng Han Sua:** Software. **Hieng Kiat Jun:** Data curation. **Yilun Liu:** Supervision, Data curation. **Yang Lu:** Writing – original draft, Supervision, Funding acquisition. **Yang Liu:** Validation, Supervision, Project administration, Investigation. **Sida Liu:** Writing – review & editing, Validation, Supervision, Project administration, Funding acquisition.

Declaration of competing interest

The authors declare the following financial interests/personal relationships which may be considered as potential competing interests.

Acknowledgements

This work was supported by a grant from the open subject of the State Key Laboratory of Solidification Processing, Northwestern Polytechnical University (No. SKLSP202403), the National Natural Science Foundation of China (No. 52471142), the National Youth Talent Program, Ministry of Industry and Information Technology of China (No. GQQNKP005), Young Talent of Lifting engineering for Science and Technology in Shandong,China (No. SDAST2024QTB027), the open subject of the State Key Laboratory of Powder Metallurgy, Central South University (No. SKLPM-KF-003), RGC Hong Kong (GRF 11200623).

Appendix A. Supplementary data

Supplementary data to this article can be found online at https://doi.org/10.1016/j.mtbio.2025.101840.

Data availability

No data was used for the research described in the article.

References

[1] M.B. Grisham, Comp. Biochem. Physiol. A: Mol. Integr. Physiol. 165 (4) (2013) 429–438, https://doi.org/10.1016/j.cbpa.2013.02.003.
[2] M. Valko, et al., Int. J. Biochem. Cell Biol. 39 (1) (2007) 44–84.
[3] C. Huang, et al., Clin. Transl. Med. 12 (11) (2022) e1094.
[4] M. Chang, T.T. Nguyen, Acc. Chem. Res. 54 (5) (2021) 1080–1093.
[5] U.S. Srinivas, et al., Redox Biol. 25 (2019) 101084, https://doi.org/10.1016/j.redox.2018.101084.
[6] Z. He, et al., J. Mater. Chem. B 9 (32) (2021) 6326–6346.
[7] K. Dong, et al., Mater. Today 20 (7) (2017) 346–353, https://doi.org/10.1016/j.mattod.2017.06.003.
[8] J.-Y. Ji, et al., Int. J. Nanomed. 17 (2022) 3163, https://doi.org/10.2147/IJN.S363827.
[9] X. Qi, et al., Adv. Mater. 35 (48) (2023) 2306632, https://doi.org/10.1002/adma.202306632.
[10] Y. An, et al., Cardiovasc. Diabetol. 22 (1) (2023) 237.
[11] J.M. Matés, et al., Clin. Biochem. 32 (8) (1999) 595–603.
[12] M. Kashif, et al., Redox Biol. 60 (2023) 102619, https://doi.org/10.1016/j.redox.2023.102619.
[13] B. D'Autréaux, M.B. Toledano, Nat. Rev. Mol. Cell Biol. 8 (10) (2007) 813–824.
[14] H. Kanzaki, et al., Front. Physiol. 8 (2017) 351.
[15] Q. Tang, et al., Adv. Funct. Mater. 31 (7) (2021) 2007475.
[16] B. Huchzermeyer, et al., Antioxidants 11 (4) (2022) 761.
[17] X. Cai, et al., Mater. Today 44 (2021) 211–228, https://doi.org/10.1016/j.mattod.2020.12.005.
[18] J. De Almeida, R. Ahuja, Phys. Rev. B Condens. Matter 73 (16) (2006) 165102, https://doi.org/10.1103/PhysRevB.73.165102.
[19] Y. Sun, et al., Nat. Commun. 12 (1) (2021) 1369.
[20] Y. Sun, et al., Adv. Mater. 34 (46) (2022) 2206208, https://doi.org/10.1002/adma.202206208.
[21] Z. Shi, et al., J. Chin. Pharmaceut. Sci. 20 (5) (2011) 498, https://doi.org/10.5246/jcps.2011.05.063.
[22] W. Feng, et al., Nat. Commun. 12 (1) (2021) 2203.
[23] M. Aureliano, et al., Int. J. Mol. Sci. 24 (6) (2023) 5382, https://doi.org/10.3390/ijms24065382.
[24] R.M. Nzietchueng, et al., J. Trace Elem. Med. Biol. 16 (4) (2002) 239–244, https://doi.org/10.1016/S0946-672X(02)80051-7.
[25] Z. Gao, et al., Biomaterials 104 (2016) 201–212, https://doi.org/10.1016/j.biomaterials.2016.06.046.
[26] X. He, et al., Mater. Today Nano 17 (2022) 100149, https://doi.org/10.1016/j.mtnano.2021.100149.
[27] B. Li, et al., Mater. Today 65 (2023) 47–61, https://doi.org/10.1016/j.mattod.2023.03.024.
[28] Y. Li, et al., Appl. Surf. Sci. 450 (2018) 284–291, https://doi.org/10.1016/j.apsusc.2018.04.205.
[29] Z. Dai, et al., Mater. Today 65 (2023) 62–77, https://doi.org/10.1016/j.mattod.2023.03.025.
[30] Z. Li, et al., Mater. Today Bio 15 (2022) 100264, https://doi.org/10.1016/j.mtbio.2022.100264.
[31] S. Cheng, et al., ACS Appl. Mater. Interfaces 14 (9) (2022) 11144–11155.
[32] Y. Guo, et al., Adv. Mater. 36 (8) (2024) 2306292, https://doi.org/10.1002/adma.202306292.
[33] Q. Zeng, et al., ACS Nano 16 (2) (2022) 1708–1733.
[34] H. Wang, et al., Adv. Healthcare Mater. 12 (8) (2023) 2202685.
[35] W. Duan, et al., Mater. Today Bio 25 (2024) 100979, https://doi.org/10.1016/j.mtbio.2024.100979.
[36] J. Liu, et al., J. Hematol. Oncol. 16 (1) (2023) 116, https://doi.org/10.1186/s13045-023-01512-7.
[37] A. Baptista, et al., Coatings 8 (11) (2018) 402.
[38] S. Mehla, et al., Catal. Sci. Technol. 9 (14) (2019) 3582–3602.
[39] W. Qing, et al., Adv. Colloid Interface Sci. 282 (2020) 102207.